Social isolation stress induces ATF-7 phosphorylation and impairs silencing of the 5-HT 5B receptor gene

Toshio Maekawa[1,6,]*, Seungjoon Kim[1,6,7], Daisuke Nakai[1,2], Chieko Makino[1,2,8], Tsuyoshi Takagi[1], Hiroo Ogura[3], Kazuyuki Yamada[4], Bruno Chatton[5] and Shunsuke Ishii[1,2,]*

[1]Laboratory of Molecular Genetics, RIKEN Tsukuba Institute, Tsukuba, Ibaraki, Japan, [2]University of Tsukuba, Graduate School of Comprehensive Human Sciences, Tsukuba, Ibaraki, Japan, [3]Tsukuba Research Laboratories, Eisai Co., Ltd, Ibaraki, Japan, [4]Support Unit for Animal Experiment, Research Resources Center, Brain Science Institute (BSI), RIKEN, Wako, Saitama, Japan and [5]Ecole Supérieure de Biotechnologie de Strasbourg, Université Louis Pasteur, Parc d'innovation, UMR7100 CNRS-ULP, Strasbourg, Illkirch Cedex, France

Many symptoms induced by isolation rearing of rodents may be relevant to neuropsychiatric disorders, including depression. However, identities of transcription factors that regulate gene expression in response to chronic social isolation stress remain elusive. The transcription factor ATF-7 is structurally related to ATF-2, which is activated by various stresses, including inflammatory cytokines. Here, we report that *Atf-7*-deficient mice exhibit abnormal behaviours and increased 5-HT receptor 5B (*Htr5b*) mRNA levels in the dorsal raphe nuclei. ATF-7 silences the transcription of *Htr5B* by directly binding to its 5′-regulatory region, and mediates histone H3-K9 trimethylation via interaction with the ESET histone methyltransferase. Isolation-reared wild-type (WT) mice exhibit abnormal behaviours that resemble those of *Atf-7*-deficient mice. Upon social isolation stress, ATF-7 in the dorsal raphe nucleus is phosphorylated via p38 and is released from the *Htr5b* promoter, leading to the upregulation of *Htr5b*. Thus, ATF-7 may have a critical role in gene expression induced by social isolation stress.

*Corresponding authors. T Maekawa or S Ishii, Laboratory of Molecular Genetics, RIKEN Tsukuba Institute, 3-1-1 Koyadai, Tsukuba, Ibaraki 305-0074, Japan. Tel.: +81 29 836 9031; Fax: +81 29 836 9030;
E-mail: maekawa@rtc.riken.jp or sishii@rtc.riken.jp
[6]These authors contributed equally to this work
[7]Present address: Laboratory of Veterinary Reproduction, Kyungpook National University, Sankyuk-dong, Buk-gu Daegu 702-701, South Korea
[8]Present address: Division of Molecular Genetics, Department of Physiology and Cell Biology, Kobe University Graduate School of Medicine, Kobe 650-0017, Japan

Introduction

ATF-7 (originally called ATFa) is structurally related to ATF-2 (Hai *et al*, 1989; Maekawa *et al*, 1989; Gaire *et al*, 1990), a member of the ATF–CREB family of transcription factors. ATF-2, ATF-7, and CRE-BPa (Nomura *et al*, 1993) form a subfamily in the ATF–CREB family. Each of these three factors contains a transcription-activation domain consisting of a metal-finger structure and stress-activated protein kinase (SAPK) phosphorylation sites, and a b-ZIP type DNA-binding domain. Various stresses, including inflammatory cytokines, activate SAPKs such as p38 and JNK (Davis, 2000), which then phosphorylate ATF-2 and activate its *trans*-activating capacity (Gupta *et al*, 1995; Livingstone *et al*, 1997; van Dam *et al*, 1997). ATF-7 is also phosphorylated by p38, but not by JNK (De Graeve *et al*, 1999). ATF-2 and ATF-7 can form homodimers or heterodimers with Jun and bind to cAMP response element (CRE) (5′-TGACGTCA-3′) (Chatton *et al*, 1994).

ATF-7 binds to mouse ATFa-associated modulator (mAM) which is a component of the ESET complex (De Graeve *et al*, 2000; Wang *et al*, 2003). As ESET is a histone methyltransferase (HMTase) that converts lysine 9 of histone H3 (H3-K9) from the dimethyl to the trimethyl form, therefore ATF-7 is thought to support gene silencing by inducing histone H3-K9 trimethylation. Two reports have suggested a role for ATF-2 family transcription factors in epigenetic gene silencing. The yeast homologue of ATF-2, Atf1, contributes to heterochromatin formation independently of the RNAi machinery (Jia *et al*, 2004). Vertebrate ATF-2 also interacts with the histone variant macroH2A, which is enriched in the inactive X chromosome in female mammalian cells and functions to maintain gene silencing (Agelopoulos and Thanos, 2006).

Both ATF-7 and ATF-2 are ubiquitously expressed in various tissues, including the brain (Takeda *et al*, 1991; Goetz *et al*, 1996). *Atf-2* null mice die immediately after birth because of defects in respiration, which appear to be caused by impaired proliferation of cytotrophoblasts in the placenta (Maekawa *et al*, 1999). *Atf-2* heterozygotes are highly prone to mammary tumours in which the expression levels of *Maspin*, a tumour suppressor, and *Gadd45α,* which is induced by hypoxic stress, are decreased (Maekawa *et al*, 2007). Both these genes encode the regulators of apoptosis, suggesting that defects in the apoptotic machinery are linked to the occurrence of mammary tumours. In contrast, the physiological role of ATF-7 is unknown, although the *Atf-2* and *Atf-7* double mutant exhibits embryonic lethality with abnormalities in the developing liver and heart (Breitwieser *et al*, 2007).

Human neuropsychiatric disorders, such as depression, have multiple-risk factors, including environmental and genetic factors. A loss of social contact is one environmental factor that appears to be linked to both the onset and relapse

of depression (Paykel *et al*, 1980). Long-term social isolation of rodents after weaning provides a model to study the behavioural consequences of loss of social interactions. Many of the symptoms induced by isolation rearing may be relevant to neuropsychiatric disorders (Rodgers and Cole, 1993). Isolated animals are aggressive and exhibit anxiety-like behaviours and increased locomotor activity (Rodgers and Cole, 1993; Blanchard *et al*, 2001). One of the typical abnormal behaviour in isolation-reared mice is a deficit in pre-pulse inhibition (PPI) of the acoustic startle response (Wilkinson *et al*, 1994). In fact, isolation-induced disruption of PPI has been used as a disease model in screening antipsychotic drugs. In animal studies, isolation stress changes the activity of brain neurotransmitters (Blanc *et al*, 1980; Blanchard *et al*, 2001). In the case of acute stress, several transcription factors, including c-Fos and corticosteroid receptors, are activated and modulate multiple target genes (Kaufer *et al*, 1998). However, the transcription factors that are activated and the regulation of gene expression patterns in response to a chronic stress, such as social isolation stress, remain elusive. In addition, as the effect of social isolation stress on behaviour is long-lived, this stress may cause epigenetic changes. However, the mechanism by which epigenetic change is caused by isolation stress remains unknown.

In this study, we have demonstrated that *Atf-7*-deficient (*Atf-7*$^{-/-}$) mice exhibit abnormal behaviours reminiscent of isolation-reared wild-type (WT) mice. Social isolation stress induced the phosphorylation of ATF-7 and p38 in the dorsal raphe nuclei, as well as a release of ATF-7 from the promoter of the 5-HT receptor 5B (*Htr5b*) gene, leading to an impaired silencing of this gene.

Results

Abnormal behaviours of Atf-7$^{-/-}$ mice

We generated *Atf-7*$^{-/-}$ mice (Supplementary Figure S1), and, under pathogen-free conditions, *Atf-7*$^{-/-}$ mice appeared healthy until at least 12 months of age. As *Atf-7* mRNA is expressed at relatively high levels in parts of the brain (Goetz *et al*, 1996), we examined various behaviours originally using WT and *Atf-7*$^{-/-}$ littermate mice with a mixed CBA (25%) × C57BL/6 (75%) genetic background, and later using C57BL/6 congenic mice. In the marble-burying test, which is used to examine anxiety-related behaviours (Spooren *et al*, 2000), *Atf-7*$^{-/-}$ mice exhibited increased marble-burying behaviour compared with WT mice (Figure 1A and Supplementary Figure S2A). In other tests of anxiety-related behaviours, such as the amount of time spent in the centre of an open-field and the elevated plus-maze test (Spooren *et al*, 2000), there was no significant difference between *Atf-7*$^{-/-}$ and WT mice (Figure 1B and C and Supplementary Figure S2B). *Atf-7*$^{-/-}$ mice did exhibit a significant increase in the startle response to a pulse-alone stimulus (Figure 1D and Supplementary Figure S2C). PPI, in which the startle reflex response is attenuated by a pre-pulse, is an important measure of sensorimotor gating (Geyer *et al*, 1990). *Atf-7*$^{-/-}$ mice displayed lower levels of PPI of the acoustic startle response (Figure 1E and Supplementary Figure S2D). Although the association between the startle response and PPI is not currently clear, a negative correlation between the startle response and PPI in WT mice has been
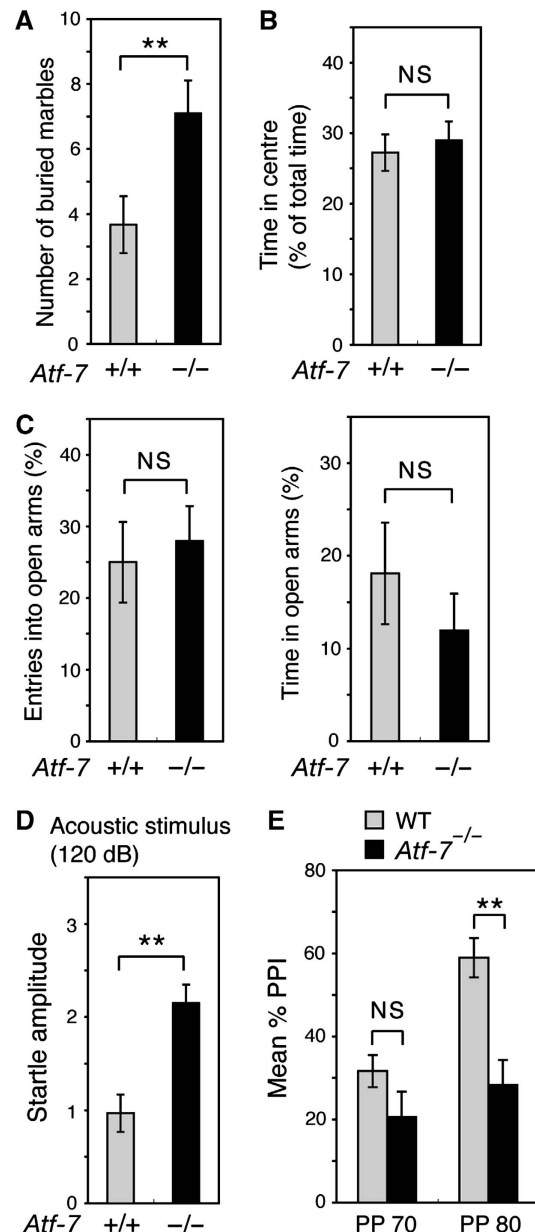

Figure 1 Abnormal behaviours in *Atf-7*$^{-/-}$ mice. Wild-type (WT; +/+) and *Atf-7*$^{-/-}$ C57BL/6 congenic mice were used for all assays. Data are mean ± s.e.m. (**A**) Marble-burying test. **P<0.01 (*n*=10–12 for each group). (**B**) Center of the open-field test. Time spent in the center of the test apparatus is expressed as a percent of total time (10 min). NS, no significant difference (*n*=13–16 for each group). (**C**) Elevated plus-maze test. Mice were observed in an elevated plus-maze for 5 min. Percentage of entries into open arms (left) and the time spent in open arms (right) are shown (*n*=13–16 for each group). (**D**) Acoustic startle response. Amplitude of the startle response to a 120 dB acoustic stimulus is shown (*n*=13–16 for each group). (**E**) Pre-pulse inhibition of the acoustic startle response. The response to a white noise stimulus of 120 dB after a 20 ms pre-pulse warning stimulus (70 or 80 dB) is shown (*n*=13–16 for each group).

reported (Egashira *et al*, 2005). If these two phenomena are correlated in *Atf7*$^{-/-}$ mice, an increase in startle reactivity may lead to decreased PPI. However, we cannot exclude the possibility that ATF-7 is independently involved in the modulation of startle response and its PPI.

The *Atf-7*$^{-/-}$ and WT mice responses were indistinguishable in other behavioural tests. We examined spontaneous locomotor activity in a new environment by placing mice in an open-field chamber and monitoring their behaviour. There was no significant difference in the locomotor activity of *Atf-7*$^{-/-}$ and WT mice on the first and second day of the trials (Supplementary Figure S3A and B). We also examined motor coordination using a rotating rod treadmill. Overall, the amount of time mice spent on the rotarod increased with training (Supplementary Figure S3C). The retention time of *Atf-7*$^{-/-}$ mice on the rod was not significantly different from that of WT mice at 0 (stationary), 5, or 10 r.p.m. In the footprint test, there was no significant difference in the stride length and the step width between mutant and WT mice (Supplementary Figure S3D).

In the forced swimming test, there was also no difference between *Atf-7*$^{-/-}$ and WT mice (Supplementary Figure S4A). We also examined spatial learning ability using the Morris Water Maze task. WT and *Atf-7*$^{-/-}$ mice took similar lengths of time to reach the visual platform to escape from the water (Supplementary Figure S4B), thus indicating that *Atf-7*$^{-/-}$ mice have normal vision, motor function, and escape behaviour in the water maze task. Mice were then trained in a hidden platform task, in which mice search for a submerged platform to escape from the water. *Atf-7*$^{-/-}$ and WT mice took similar lengths of time over the 7 days of testing to locate the hidden platform (Supplementary Figure S4C). Thus, *Atf-7*$^{-/-}$ and WT mice were able to learn the location of a hidden platform during the course of the trials. We then carried out a probe test, in which the platform is removed from the pool after completion of the hidden platform task, and the trained mice are allowed to swim freely for 60 s. The time spent in the target quadrant by *Atf-7*$^{-/-}$ mice was similar to that of WT mice (Supplementary Figure S4D). These results indicate that a normal spatial learning ability is present in *Atf-7*$^{-/-}$ mice. The number of crossings of the hidden platform and the swimming distance of *Atf-7*$^{-/-}$ and WT mice was also similar during the probe trial (Supplementary Figure S4E and F). Thus, the performance of *Atf-7*$^{-/-}$ mice in the hidden platform task was indistinguishable from WT mice.

Upregulation of the Htr5b gene in the dorsal raphe nucleus of Atf-7$^{-/-}$ mice

Atf-7 mRNA was detected in the cortex, the cerebellum, the hippocampus, and the brainstem, including the medulla, the pons, and the midbrain of WT mice (Figure 2A), but not of *Atf-7*$^{-/-}$ mice (Supplementary Figure S5). No obvious morphological abnormalities were found in these tissues in *Atf-7*$^{-/-}$ mice (data not shown). Western blotting indicated that ATF-7 expression levels varied in these tissues (Figure 2B). Several studies have linked abnormal marble-burying behaviour to 5-HT function (Jenck *et al*, 1998). Further, disruptions in PPI of the startle response are correlated not only with D2 dopamine and *N*-methyl-D-aspartate signalling systems, but also with 5-HT (Geyer *et al*, 2001). Therefore, we focused our attention on the dorsal raphe nuclei of the brainstem, where much of the 5-HT in the brain is localized and relatively high levels of ATF-7 are expressed.

To identify the ATF-7 target genes in the brainstem that may have a role in the abnormal behaviour in *Atf-7*$^{-/-}$ mice, we performed a DNA microarray analysis using RNA from the brainstem of *Atf-7*$^{-/-}$ and WT mice. The results indicate that 25 genes were upregulated and 38 genes downregulated by more than two-fold by the loss of *Atf-7*. Of these ATF-7 target genes, the functions of 11 of the upregulated genes are known, whereas the functions of only 7 of the downregulated genes have been reported. Among these genes, only the *Htr5b* and the ciliary neurotrophic factor receptor (*Cntfr*) genes have been associated with neuronal function. As the 5-HT system appeared to be associated with the abnormal behaviour of *Atf-7*$^{-/-}$ mice as described above, upregulation of the *Htr5b* gene may be associated with the phenotype of *Atf-7*$^{-/-}$ mice. CNTF is a cytokine that has neurotrophic and differentiating effects on cells in the central nervous system, and the CNTF–CNTF receptor system affects motor neurons (Vergara and Ramirez, 2004). However, there has been no report demonstrating a connection between the CNTF system and anxiety-related behaviours. Therefore, we focused our attention on the *Htr5b* gene.

As Htr5b is thought to act as an autoreceptor (Serrats *et al*, 2004), its upregulation may lead to a decrease in the extracellular concentration of serotonin (5-HT). There is abundant evidence for the role of decreased 5-HT in depression and anxiety disorders (Artigasa *et al*, 1996). Selective serotonin re-uptake inhibitors (SSRIs), which increase the extracellular concentration of 5-HT in the dorsal raphe nuclei, are widely used as anti-depressant drugs. *Htr5b* mRNA levels in the *Atf-7*$^{-/-}$ brainstem were approximately 12-fold higher than in WT (Figure 2C). *In situ* hybridization showed higher levels of *Htr5b* mRNA expression in the *Atf-7*$^{-/-}$ dorsal raphe nuclei, which also expressed a serotonin transporter mRNA, than in the WT (Figure 2D and Supplementary Figure S6). There appeared to be no obvious difference in the levels of *Htr5b* mRNA between WT and *Atf-7*$^{-/-}$ mice in other regions, including the hippocampus, the habenular nucleus, and the inferior olivary nucleus (Supplementary Figure S7).

Among the many reported antagonists of 5-HT receptors, methiothepin has a relatively high affinity for the 5-HT 5B receptor, although it also binds to other 5HT receptors, including the 5-HT 1A receptor (Boess and Martin, 1994). Injection of methiothepin into *Atf-7*$^{-/-}$ mice suppressed the increased marble-burying behaviour, whereas saline-treated control *Atf-7*$^{-/-}$ mice still exhibited increased marble-burying behaviour (Figure 2E). Furthermore, methiothepin also alleviated the lower levels of PPI in *Atf-7*$^{-/-}$ mice (Figure 2F). These results suggest that increased expression of *Htr5b* mRNA in the *Atf-7*$^{-/-}$ brainstem may, at least partly, contribute to their abnormal behaviour, although loss of ATF-7 could cause changes in the expression of other genes in various regions of the brain and also contribute to abnormal behaviours.

Silencing of the Htr5b gene by ATF-7 via direct binding to its 5′-region

Analysis of the DNA sequence in the 5′ region of the mouse *Htr5b* gene identified three CRE-like sites at nucleotides -3374, -3340, and -2325 (where $+1$ is the major transcriptional start site), all of which have only a 1 or 2 bp difference from the consensus CRE sequence (Figure 3A). Gel mobility-shift assays were carried out using nine DNA probes, which cover approximately 4.4 kbp of the 5′-region of *Htr5b*, and nuclear extracts from 293T cells that were transfected with a Flag-tagged ATF-7 expression plasmid or control
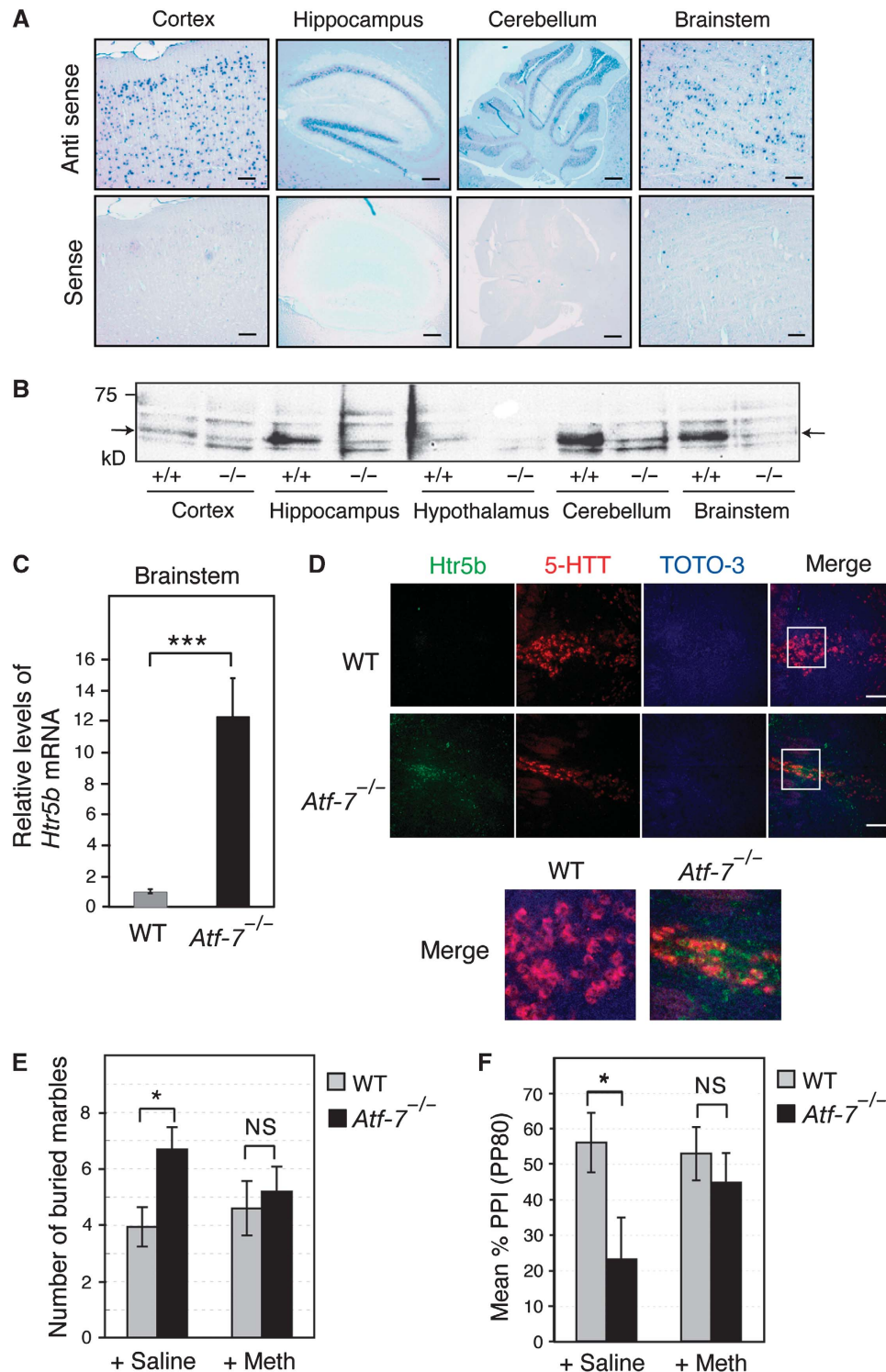
Figure 2 Increased levels of *5-HT receptor 5B* (*Htr5b*) mRNA in the *Atf-7⁻/⁻* brainstem. (**A**) *Atf-7* mRNA expression in various regions of the brain was examined by *in situ* hybridization with anti-sense and sense probes. Bar, 100 μm. (**B**) Extracts (20 μg of protein) from the indicated regions of wild-type (WT) or *Atf-7⁻/⁻* brains were used for western blotting with anti-ATF-7. The bands indicated by arrows are the ATF-7 signals. (**C**) Real-time RT–PCR analysis of *Htr5b* mRNA levels using total RNA from the brainstem ($n = 4$). ***$P < 0.001$. (**D**) *Htr5b* mRNA expression in the dorsal raphe nuclei was examined by *in situ* hybridization using probes for *Htr5b* (green) and the serotonin transporter (5-HTT, red). Cell nuclei were identified by DNA staining using TOTO-3 (blue). The sections were examined by laser confocal microscopy, and representative images are presented. The panels at the right show the merged images. Bar, 100 μm. The white box indicates a subregion of each image that is presented at higher magnification below. (**E, F**) A 5-HT 5B receptor antagonist reduced the abnormal behaviour of *Atf-7⁻/⁻* mice. Marble-burying behaviour (E) and pre-pulse inhibition (PPI) (F) of WT and *Atf-7⁻/⁻* C57BL/6 congenic mice was examined after administration of either vehicle or methiothepin ($n = 10-12$ for each group in E, and $n = 7$ for each group in F). *$P < 0.05$.
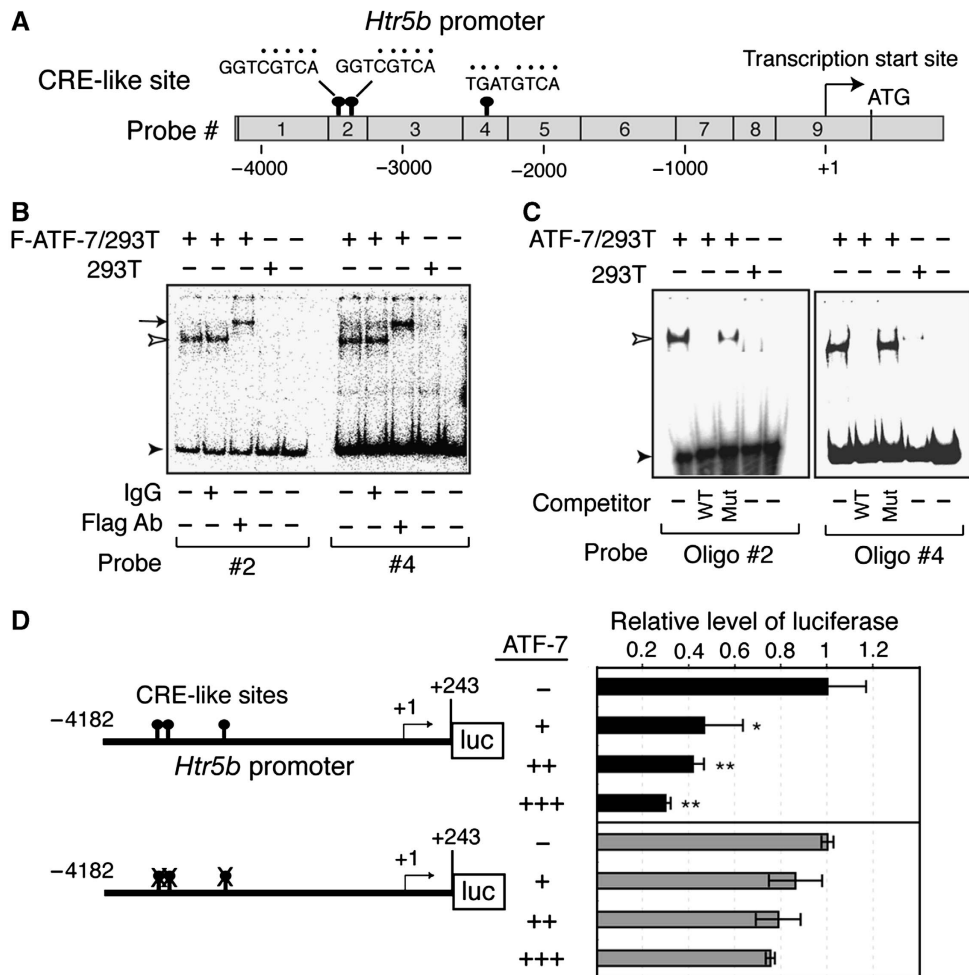
Figure 3 Binding of ATF-7 to the *5-HT receptor 5B* (*Htr5b*) promoter region leads to silencing. (**A**) Presence of cAMP response element (CRE)-like sites in the 5′ region of the mouse *Htr5b* gene. The CRE-like sites in the 5′-region of mouse *Htr5b*, and nine DNA probes used for gel mobility-shift assays are shown. (**B, C**) Gel mobility-shift assays were performed using nuclear extracts prepared from 293T cells transfected with a Flag-ATF-7 expression vector or control empty vector. The #2 and #4 DNA probes were used as the probes in (B). In some lanes, anti-Flag or control IgG was added. In (C), oligonucleotides containing the two CRE-like sites derived from probe #2 or the one CRE-like site from probe #4 were used as probes. In some lanes, a 50-fold excess of competitor containing the same sequence as the probe (wild-type (WT)), or a mutated CRE-like site, was added. Free probe is indicated by a closed arrowhead, whereas ATF-7-bound DNA is shown by an open arrowhead. The ATF-7-DNA complex, which was super-shifted by the anti-Flag antibody, is indicated by the arrow. (**D**) ATF-7 represses *Htr5b* gene transcription. RN46A cells were transfected with the indicated *Htr5b* promoter-luciferase construct together with 1 (+), 2 (++), or 3 (+++) µg of the ATF-7 expression plasmid, or the control empty vector (−), and luciferase activity was measured. Values indicate mean ± s.d. ($n = 3$). *$P < 0.05$, **$P < 0.01$.

empty vector. When the #2 or #4 probes were used, a retarded band was detected in extracts containing Flag-ATF-7 (Figure 3B). These specific retarded bands were further shifted when an anti-Flag antibody was added, indicating that the bands contained Flag-ATF-7. In contrast, no retarded bands were observed with the other probes (Supplementary Figure S8). We then used 54 bp and 18 bp oligonucleotides containing the CRE-like sites derived from the #2 and #4 probes, respectively. The retarded bands generated using either probe were competed out by excess amounts of un-labelled competitor oligonucleotide, but not by competitors, which contained mutated CRE-like sites (Figure 3C). These results indicate that ATF-7 binds directly to the CRE-like sites in the 5′-region of the mouse *Htr5b* gene.

When a *Htr5b* promoter-luciferase reporter containing the 4.4 kb 5′-region of the *Htr5b* gene was cotransfected into RN46A cells, which are derived from rat medullary raphe nucleus cells, ATF-7 inhibited luciferase expression by ap-proximately 70% (Figure 3D). In contrast, mutation of the three CRE-like sites in this reporter relieved the ATF-7-dependent silencing. These results suggest that ATF-7 sup-presses the transcription of *Htr5b* through interaction with CRE-like sites.

The results of chromatin immunoprecipitation (ChIP) as-says using the brainstem chromatin and an anti-ATF-7 anti-body indicated that ATF-7 bound to the region containing CRE-like sites of the *Htr5b* gene, but not to the RNA start site or the 2nd exon (Figure 4A). Further, the binding of ATF-7 to this region was not detected using the *Atf-7*$^{−/−}$ brainstem chromatin. Binding of ATF-2 to this region was also not detected (Figure 4B).

ATF-7 mediates histone H3-K9 trimethylation of the Htr5b promoter region by recruiting the ESET HMTase

The results of ChIP assays using the WT brainstem chromatin and anti-H3-K9m3 antibodies indicated that histone H3 in the
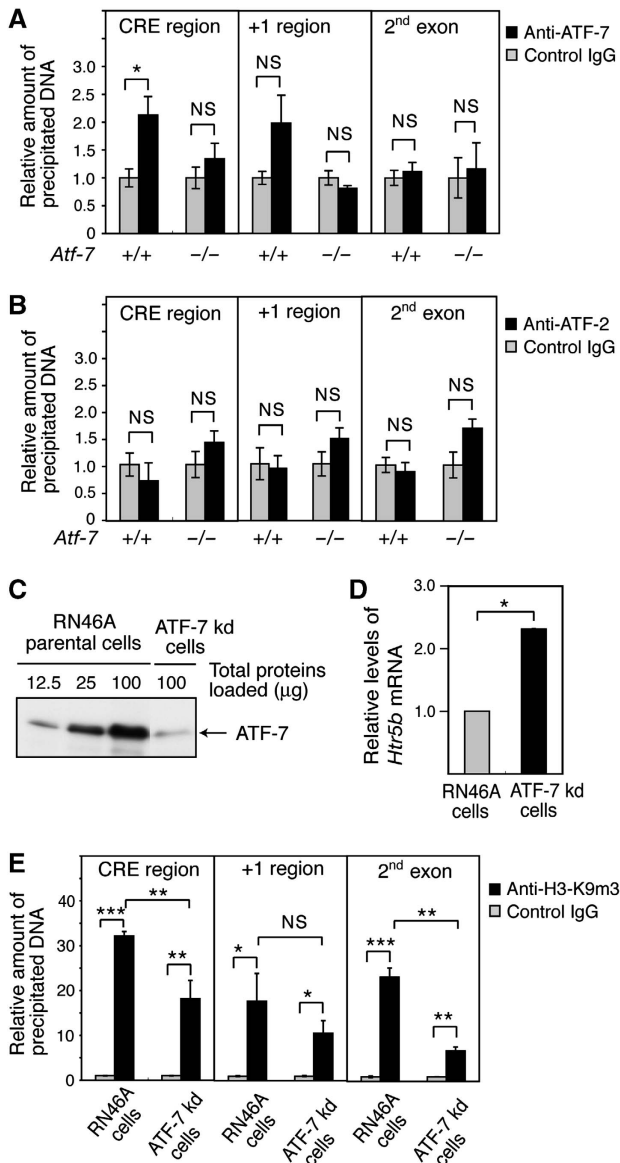
Figure 4 Binding of ATF-7 to the *5-HT receptor 5B* (*Htr5b*) promoter is correlated with histone H3-K9 trimethylation. (**A, B**) Chromatin immunoprecipitation (ChIP) assays were carried out using the brainstem of wild-type (WT) and *Atf-7*−/− mice, and anti-ATF-7 (A), anti-ATF-2 (B), or control IgG (A, B). Extracted DNA was amplified by real-time PCR using primers that cover the cAMP response element (CRE)-like sites, the transcription start site, or the 2nd exon of the *Htr5b* gene. The relative densities of bands are indicated, and each bar represents the mean ± s.d. (*n* = 3). (**C**) Generation of an RN46A cell line in which ATF-7 levels are downregulated (ATF-7 kd-RN46A) by expression of a small hairpin-type double-stranded RNA. Nuclear extracts of the parental RN46A cells and the ATF-7 kd-RN46A cells were used for western blotting to detect ATF-7. (**D**) Real-time RT–PCR analysis of *Htr5b* mRNA levels using RNAs from the parental RN46A cells and ATF-7 kd-RN46A cells. Values are mean ± s.d. (*n* = 3). (**E**) ChIP assays were carried out using anti-histone H3-K9m3 and parental RN46A cells or ATF-7 kd-RN46A cells. Extracted DNA was amplified by real-time PCR using primers that cover the CRE-like sites, the transcription start site, or the 2nd exon of the *Htr5b* gene. The relative densities of the bands are indicated, and each bar represents the mean ± s.d. (*n* = 3). *$P < 0.05$, **$P < 0.01$, ***$P < 0.001$.

region containing the CRE-like sites, the RNA start site, and the 2nd exon of *Htr5b* is trimethylated at K9 (Supplementary Figure S9A). When the *Atf-7*−/− brainstem chromatin was used, similar levels of histone H3-K9 trimethylation were

detected. This result may indicate that *Htr5b* gene transcription is repressed by histone methylation in most cells of the brainstem with the exception of the dorsal raphe nucleus in *Atf-7*−/− mice. To assess the role of ATF-7 in histone H3-K9 methylation, we generated an ATF-7 knock-down (kd) RN46A cell line by expressing a small hairpin-type double-strand RNA. The ATF-7 level was approximately one-eighth that of the parental cell line (Figure 4C). In kd-RN46A cells, *Htr5b* mRNA levels increased approximately 2.3-fold compared with the parental cell line (Figure 4D). In ChIP assays, binding of ATF-7 to the region containing the CRE-like sites of the *Htr5b* gene was detected in parental RN46A cells, but not in the ATF-7 kd-RN46A cells (Supplementary Figure S9B). Binding of ATF-2 to the same region was not detected (Supplementary Figure S9C). The degree of histone H3-K9 trimethylation in the region containing the CRE-like sites or the 2nd exon of *Htr5b* gene was lower in the kd-RN46A cells than in parental cells (Figure 4E). Thus, ATF-7 contributes to H3-K9 trimethylation at the *Htr5b* gene promoter.

To investigate whether the ESET HMTase is involved in the silencing of *Htr5b* by ATF-7, we examined ATF-7–ESET interactions by co-immunoprecipitation. Immunocomplexes prepared from RN46A cell lysates using anti-ATF-7 contained ESET, whereas immunocomplexes prepared with control IgG did not contain ESET (Figure 5A). The results of ChIP assays using the WT brainstem chromatin and anti-ESET antibodies indicated that ESET bound to the region containing CRE-like sites of *Htr5b*, but not to the region containing the RNA start site or the 2nd exon (Figure 5B). Further, binding of ESET to this region was not detected using the *Atf-7*−/− brainstem chromatin. Similar results were also obtained in ChIP assays using the parental RN46A and ATF-7 kd-RN46A cells (Figure 5C).

Members of the ATF-2 subfamily are activated in response to various stresses, and TNF-α is one of the typical inflammatory cytokines which can activate ATF-2 (Brinkman *et al*, 1999). When RN46A cells were treated with TNF-α, the level of *Htr5b* mRNA was gradually increased, by approximately 2.5-fold at 8 h after TNF-α addition (Figure 5D). Phosphorylation of ATF-7 at Thr-53 and of ATF-2 at Thr-71 was also enhanced by TNF-α treatment (Figure 5E). The gradual increase in ATF-7 and ATF-2 phosphorylation observed here is apparently different from the rapid and transient induction of ATF-2 phosphorylation in response to osmotic stress and TGF-β treatment in non-neuronal cells, in which ATF-2 phosphorylation peaks at 30 min after treatment and then decreases (Sano *et al*, 1999). TNF-α also rapidly induces phosphorylation of ATF-2, within 1 h in non-neuronal cells (Brinkman *et al*, 1999). Thus, the gradual response of the p38-ATF-2/7 pathway to TNF-α may be characteristic of neurons. Furthermore, the results of ChIP assays using TNF-α-treated RN46A cells indicate that ATF-7 was released from the 5′-region of *Htr5b* by TNF-α treatment (Figure 5F).

Social isolation stress induces abnormal behaviours similar to those of *Atf-7*−/− mice and *Htr5b* expression

Defects in PPI attenuation of the acoustic startle response are induced by social isolation stress (Wilkinson *et al*, 1994), although isolated animals exhibit a variety of phenotypes, including aggressive behaviour (Blanchard *et al*, 2001). This observation suggests that exposure of WT mice to social
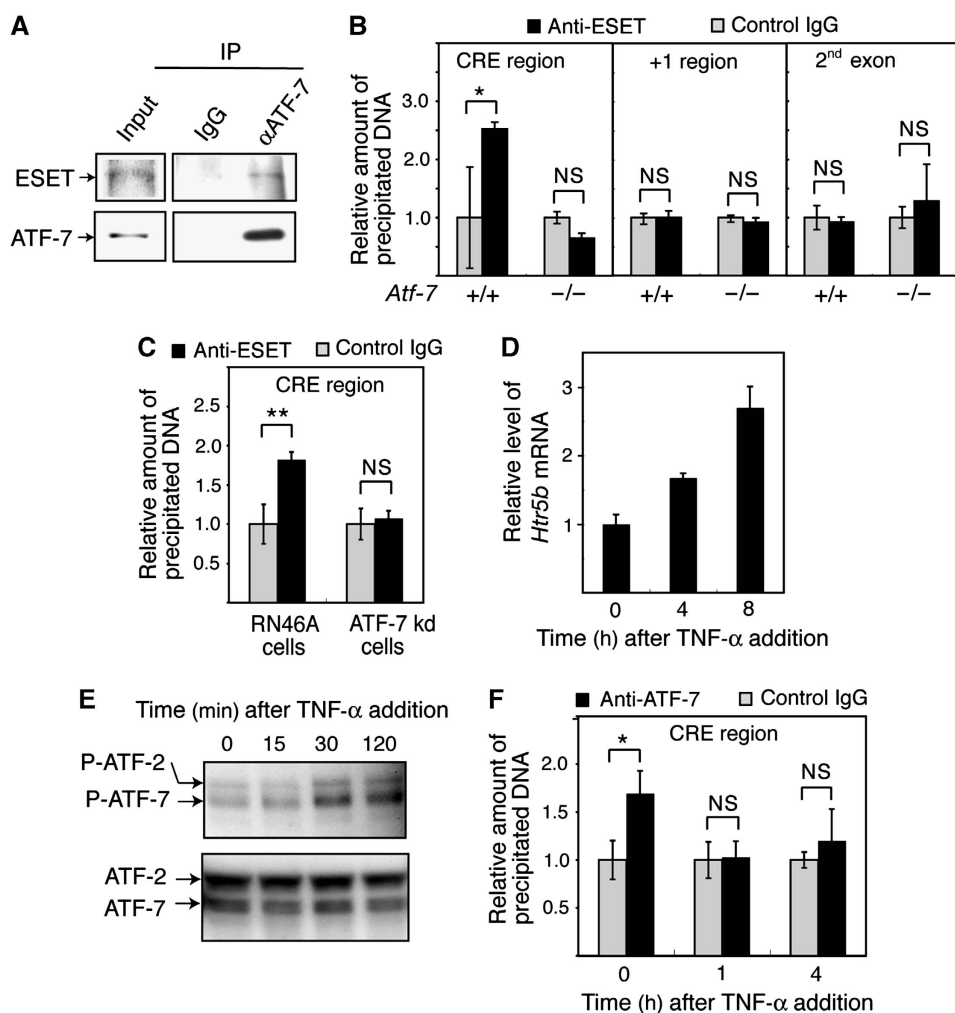
Figure 5 ATF-7 recruits the ESET HMTase to the *5-HT receptor 5B* (*Htr5b*) gene. (**A**) Co-immunoprecipitation of ATF-7 and ESET. Whole cell lysates of RN46A cells were immunoprecipitated with anti-ATF-7 or control IgG, and the immunocomplexes were then analyzed by western blotting using anti-ESET or anti-ATF-7 antibodies. (**B**) Recruitment of ESET to the *Htr5b* gene by ATF-7. Chromatin immunoprecipitation (ChIP) assays were carried out using anti-ESET and chromatin from wild-type (WT) or *Atf-7*$^{-/-}$ brainstems. Extracted DNA was amplified by real-time PCR using primers that cover the cAMP response element (CRE)-like sites, the RNA start site, or the 2nd exon of the *Htr5b* gene. The relative densities of the bands are indicated, and each bar represents the mean ± s.d. ($n = 3$). (**C**) ChIP assays were carried out using anti-ESET and the parental RN46A or the ATF-7 kd-RN46A cells. Extracted DNA was amplified by real-time PCR using primers that cover the ATF-7-binding sites of the *Htr5b* gene ($n = 3$). (**D**) Upregulation of *Htr5b* mRNA by TNF-α in RN46A cells. Real-time RT–PCR analysis of *Htr5b* mRNA was performed using RNAs from RN46A cells treated with TNF-α for the indicated times ($n = 3$). (**E**) Increase in phosphorylation of ATF-7 in response to TNF-α. Nuclear extracts were prepared from RN46A cells treated with TNF-α for the indicated times, and used for western blotting with antibodies that recognize the indicated proteins. We have identified the ATF-7 band by confirming that it was lost in the *Atf-7*$^{-/-}$ whole brain nuclear extract (Supplementary Figure S10). (**F**) Release of ATF-7 from the *Htr5b* promoter by TNF-α treatment. ChIP assays were carried out as described above using anti-ATF-7 and RN46A cells treated with TNF-α for the indicated times ($n = 3$). *$P < 0.05$, **$P < 0.01$.

isolation stress may cause abnormal behaviour and an increase in *Htr5b* mRNA levels in the dorsal raphe nuclei, both of which were observed in *Atf-7*$^{-/-}$ mice. In fact, WT mice exhibited increased marble-burying behaviour after 1 month of isolation rearing (Figure 6A). Furthermore, after isolation rearing of WT mice for 1 month, *Htr5b* mRNA levels in the brainstem increased approximately 12-fold (Figure 6B). *In situ* hybridization indicated that the level of *Htr5b* mRNA in the dorsal raphe nuclei, which also expressed serotonin transporter mRNA, was enhanced by isolation rearing (Figure 6C and Supplementary Figure S6C). The result of ChIP assays using the brainstem from group- or isolation-reared mice indicated that the degree of histone H3-K9 trimethylation was not affected by isolation stress (Supplementary Figure S11). This result may indicate that *Htr5b* gene transcription is repressed by histone methylation

in most brainstem cells with the exception of the dorsal raphe nucleus in isolation-reared mice.

When *Atf-7*$^{-/-}$ mice were exposed to isolation stress, enhancement of marble-burying behaviour was observed (Figure 6D). However, *Htr5b* mRNA levels in the *Atf-7*$^{-/-}$ brainstem were not further increased by isolation stress (Figure 6E). These results suggest that isolation stress induces abnormal marble-burying behaviour not only by induction of *Htr5b* but also by changing the expression of other genes.

Social isolation stress induces the phosphorylation of ATF-7 and release of ATF-7 from the Htr5b gene

We examined phosphorylated ATF-7 (P-ATF-7) signals in the dorsal raphe nucleus of group- and isolation-reared WT mice. Social isolation stress significantly increased the number of
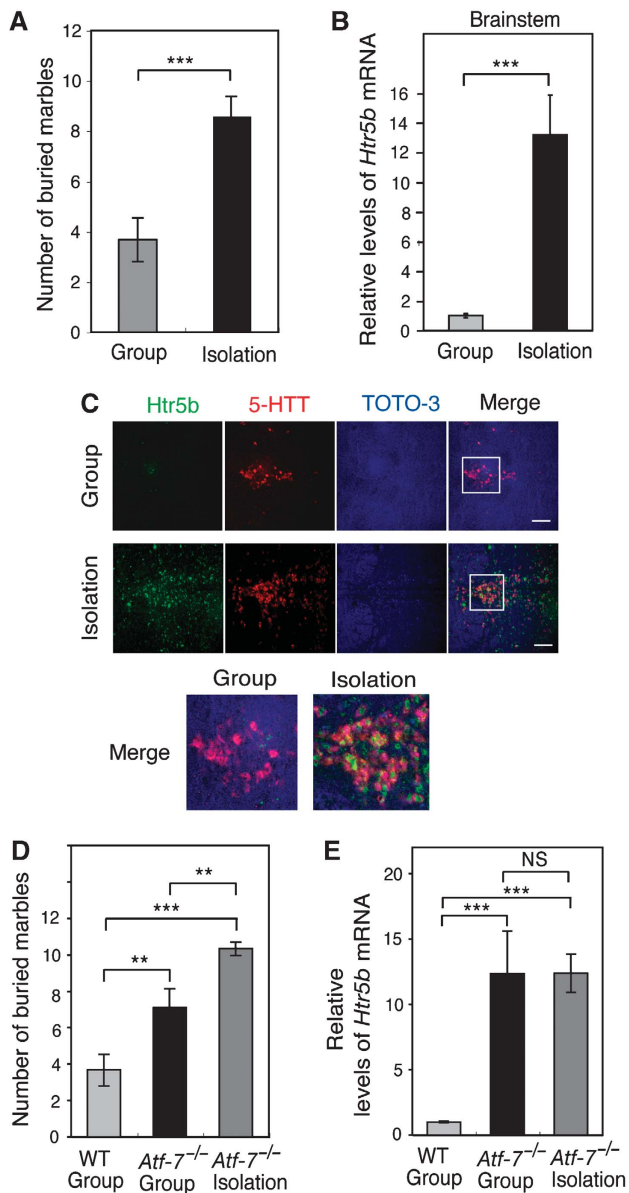
Figure 6 Social isolation stress increases marble-burying behaviour and induces *5-HT receptor 5B* (*Htr5b*) mRNA expression. (**A**) Marble-burying behaviour of group- and isolation-reared WT mice was examined ($n = 10–12$ of C57BL/6 congenic mice for each group). (**B**) Real-time RT–PCR analysis of *Htr5b* mRNA was performed using RNAs from the brainstem of group- and isolation-reared WT mice ($n = 3$). (**C**) *Htr5b* mRNA expression in the dorsal raphe nuclei of group- and isolation-reared WT mice was examined by *in situ* hybridization, as described in Figure 2D. (**D**) The group-reared WT and *Atf-7*$^{-/-}$ mice, and the isolation-reared *Atf-7*$^{-/-}$ mice were used for marble-burying tests ($n = 10–12$ of C57BL/6 congenic mice for each group). (**E**) Real-time RT–PCR analysis of *Htr5b* mRNA was performed using RNAs from the brainstems of the mice described in D ($n = 3$). $**P < 0.01$, $***P < 0.001$.

neurons expressing P-ATF-7 and P-ATF-2 in the dorsal raphe nucleus (Figure 7A). As the amino-acid sequence of the p38 phosphorylation site is highly conserved between ATF-7 and ATF-2, antibodies to P-ATF-7 also recognize P-ATF-2. However, the results of western blotting using extracts from the brainstem indicated that the phosphorylation of ATF-7 increased under social isolation stress conditions, whereas the phosphorylation of ATF-2 did not (Figure 7B). The results

of ChIP assays using the brainstem chromatin of group- and isolation-reared WT mice, and anti-ATF-7, indicated that binding of ATF-7 to the 5′-region of *Htr5b* was lost by social isolation stress (Figure 7C). These data suggest that social isolation stress induces a release of ATF-7 from the *Htr5b* promoter. Social isolation stress also significantly increased the number of neurons expressing phosphorylated, active p38 in the dorsal raphe nuclei (Figure 7D).

Discussion

This study suggests that ATF-7 may contribute to the formation of a heterochromatin-like structure in the *Htr5b* promoter via histone H3-K9 trimethylation. The effect of isolation-rearing on behaviour is long-lived, suggesting that epigenetic changes may have occurred. In the absence of stress, silencing of *Htr5b* may be maintained via ATF-7-mediated histone H3-K9 trimethylation. Phosphorylation of ATF-7 may disrupt interactions with histone methyltransferase and enhance the association with co-activators containing histone acetyltransferase and/or histone demethylase, leading to disruption of the heterochromatin-like structure. The resulting transcriptionally active chromatin structure may be stable for a relatively long time. Mechanisms by which transcriptionally active memory can be modulated without affecting DNA methylation remain elusive, but a recent report showed that the epigenetic memory of an active state can be established by histone H3.3 deposition (Ng and Gurdon, 2008).

Although at present the mechanism by which isolation stress induces phosphorylation of ATF-7 is unknown, isolation stress increases the peripheral tissue levels of TNF-α (Wu *et al*, 1999), which may move into the brain and be involved in the onset of depression (Connor and Leonard, 1998). Both isolation stress and TNF-α increased ATF-7 phosphorylation and *Htr5b* mRNA levels, which are accompanied by a release of ATF-7 from the *Htr5b* promoter. The mechanism by which the phosphorylation of ATF-7 causes a release of ATF-7 from target sites is unknown. The phosphorylation-induced release of ATF-7 from DNA could be caused by changes in interactions between ATF-7 and uncharacterized factors that enhance ATF-7 affinity for DNA. ATF-7 is highly homologous to ATF-2, but there are differences between the two proteins. In luciferase reporter assays, ATF-2 activated transcription from the CRE-containing promoter, but ATF-7 did not, even in the presence of active p38. This result suggests that ATF-7 may have a role primarily in transcriptional repression. As we have observed that ATF-7 forms a heterodimer with ATF-2 (data not shown), further study is required to compare the function of ATF-7 and ATF-2 homodimers and ATF-7–ATF-2 heterodimers.

Our results suggest that upregulation of *Htr5b* may partly contribute to the abnormal behaviour of *Atf-7*$^{-/-}$ mice. The rodent 5-HT5 receptor family consists of two receptors, 5-HT 5A and 5B (Htr5a and Htr5b), which share 69% amino acid identity and have 23–34% homology with other 5-HT receptors (Plassat *et al*, 1992). Htr5a has been identified in mouse, rat, and human. Mouse and rat have a functional Htr5b gene, whereas the human coding sequence is interrupted by stop codons (Grailhe *et al*, 2001). Thus, humans do not have a functional Htr5b, and, therefore, another subtype, such as Htr5a, could be upregulated and has a role in response to social isolation stress in humans. *Htr5a*-deficient mice
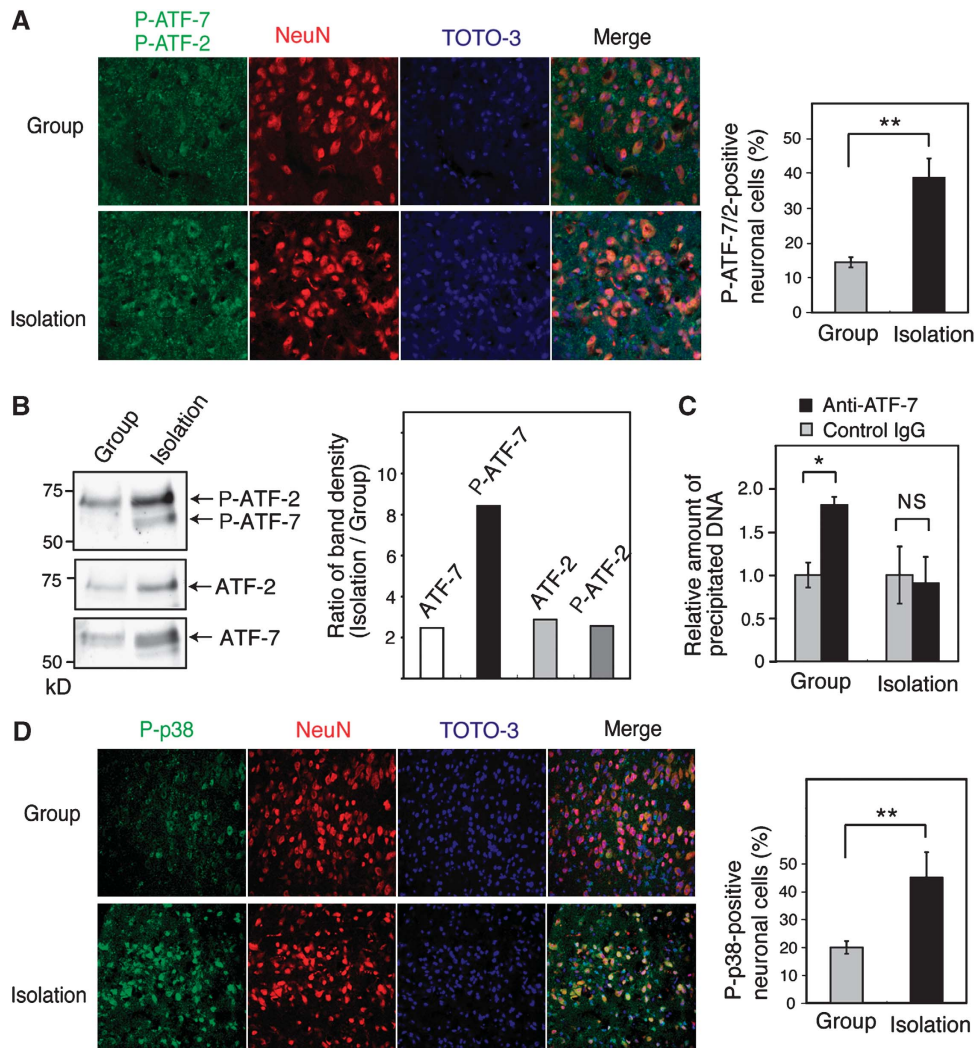
Figure 7 Social isolation stress induces ATF-7 phosphorylation and release of ATF-7 from the *5-HT receptor 5B* (*Htr5b*) promoter. (**A**) Brain sections containing dorsal raphe nuclei of group- or isolation-reared wild-type (WT) mice were stained with antibodies which recognize P-ATF-7 and P-ATF-2 (green), or NeuN (red), a neuronal specific nuclear protein. DNA was stained with TOTO-3 (blue). The merged images are shown in the right panels. The average number of neurons expressing P-ATF-7 or P-ATF-2 in three independent experiments is indicated by the bar graph ± s.d. (**B**) Nuclear extracts were prepared from the brainstem of group- or isolation-reared mice, which were perfused with PFA, and analyzed by SDS–PAGE after decrosslinking, followed by western blotting with anti-P-ATF-2/7, anti-ATF-7, and anti-ATF-2. The ratio of the density of each band in isolation-reared mice to that in group-reared mice is indicated in the bar graph. (**C**) Release of ATF-7 from the *Htr5b* promoter by isolation stress. Chromatin immunoprecipitation (ChIP) assays were carried out using chromatin from the brainstem of group- or isolation-reared WT mice, and anti-ATF-7. Extracted DNA was amplified by real-time PCR using primers that cover the ATF-7-binding sites of *Htr5b* (*n* = 3). (**D**) Brain sections containing dorsal raphe nuclei of group- or isolation-reared WT mice were stained with antibodies that recognize P-p38, as described above. The number of neurons expressing P-p38 is quantified at the right (*n* = 3). *$P < 0.05$, **$P < 0.01$.

display increased exploratory activity when exposed to new environments, suggesting that Htr5a modulates the activity of neural circuits involved specifically in exploratory behaviour (Grailhe *et al*, 1999). However, there has been no report of a mouse knockout of *Htr5b*.

Isolation-rearing was recently reported to reduce (27.0–60.9%) transcription of many postsynaptic 5-HT receptors in the prefrontal cortex and the 5-HT 1B, 2A, and 2C receptors in the hypothalamus and the midbrain, whereas 5-HT 6 receptor mRNA levels increased (52.5%) in the hippocampus (Bibancos *et al*, 2007). *Htr5b* expression was not examined. The fold change in mRNA level of these 5-HT receptors was much lower than the change in *Htr5b* mRNA described herein (12-fold). We have also examined the expression level of 5-HT receptors other than 5B in *Atf-7*$^{-/-}$

mice. Slight decreases in the 2A and 2C receptors in the hypothalamus and 1A and 1B receptors in the cortex were observed in *Atf-7*$^{-/-}$ mice, whereas the levels of 2A and 3A receptors in the cortex increased slightly (Supplementary Figure S12). However, the degree of these changes was much lower than the change in *Htr5b* in the brainstem in response to social isolation rearing. There was no difference in the *Htr5b* mRNA levels in the hypothalamus and in the cortex between WT and *Atf-7*$^{-/-}$ mice. Thus, the degree of change in the *Htr5b* mRNA levels in the brainstem in response to loss of ATF-7 or social isolation stress is dramatic, suggesting a unique role for Htr5b. However, it is also likely that loss of ATF-7 changes the expression of multiple genes in various regions of the brain that may also contribute to abnormal behaviours.

Materials and methods

Animals

All mice used were 2–6-month-old males. In the original behaviour tests, immunohistochemistry, RNA analysis, and ChIP assays, the littermate mice, which were generated by mating *Atf-7* heterozygotes with a mixed CBA (25%) × C57BL/6 (75%) genetic background, were used. To confirm some behavioural abnormalities of *Atf-7*$^{-/-}$ mice, C57BL/6 congenic mice, which were generated by backcrossing onto a C57BL/6 genetic background for 7 generations, were used. Both WT and *Atf-7*$^{-/-}$ mice were maintained in a temperature and humidity-controlled room with free access to food and water. Animals were maintained on a 12-h-light and 12-h-dark cycle (lights on at 0800 h, lights off at 2000 h). For social isolation stress, mice were group-housed until 1-month old and then housed individually for 1 month before the start of the experiments. Experiments were conducted in accordance with the guidelines of the Animal Care and Use Committee of the RIKEN Institute.

Behavioural analysis

Marble-burying test. The marble-burying behaviour tests were carried out using C57BL/6 congenic mice (Figures 1A and 2E) or mice with a mixed CBA (25%) × C57BL/6 (75%) genetic background (Supplementary Figure S2A) as described (Yamada *et al*, 2002). The mice were placed individually in plastic cages (20 × 14 × 22 cm³) for 30 min (habituation trial) and then returned to their home cages. Twelve clean, coloured glass marbles (10 mm in diameter) were evenly spaced 3–5 cm apart on 5 cm deep sawdust in the habituation cages. Mice were then re-introduced into these cages without food and water (each test mouse was returned to the same cage in which they had been habituated). The results of marble-burying behaviour were expressed as the number of marbles, at least, two-thirds buried within 30 min.

Acoustic startle response. The acoustic startle response was measured using specific startle chambers (O'Hara & Co. in Figure 1D and E, or SR-LAB, San Diego Instruments in Supplementary Figure S2C and D). The startle chamber consisted of a Plexiglas cylinder 3.5 or 3.8 cm in diameter, resting on a sensor block or on a Plexiglas frame in a sound-attenuated, ventilated enclosure. Acoustic bursts were presented through a loudspeaker mounted 25 or 29 cm above the cylinder. A piezoelectric transducer mounted below the sensor-block/frame detected motion of the animal in the cylinder. Stabilimeter readings were rectified and recorded by a microcomputer and interface ensemble (O'Hara & Co. or San Diego Instruments). One mouse was placed in each chamber and allowed to acclimate for 10 min and then the experimental session was started. Background noise was set at 65 dB white noise throughout both the acclimation period and the session. In a session, 10 trials for three types of stimuli each (total of 30 trials) were given in pseudo-random order after three initial startle-stimuli (20-ms burst of 120 dB white noise), which were given to avoid the effect of high responses to initial stimulations in the experiments. One type of trial was a pulse-alone (P alone) trial, which involved a 20-ms burst of 120 dB white noise, and the other two types of trials were pre-pulse and pulse (PP70 & P and PP80 & P) trials, in which a 20-ms burst of 70 or 80 dB white noise, respectively, was followed by a 20-ms burst of 120 dB white noise 100 ms later. The inter-trial intervals averaged 40 s (20–60 s) and were pseudo-randomized. The startle response was measured for 300 ms (Figure 1D and E) or 100 ms (Supplementary Figure S2C and D) from the beginning of pulse presentation, and the largest value was defined as the startle amplitude. The startle amplitudes of the animal in response to repetitions of each trial type were averaged across the session. The experimental schedule was controlled by a micro-computer.

Methiothepin treatment. Methiothepin mesylate salt (Sigma-Aldrich) (0.1 mg/kg weight) and saline (Otsuka) were administered by intra-peritoneal injection. Tests were conducted 1 h after drug administration.

Histological analysis and immunohistochemistry

Tissues were fixed by perfusion with 4% PFA, dehydrated, and embedded in paraffin. Sections (5 μm) were stained with hematoxylin and eosin according to standard procedures. Frozen sections (10 μm) were used for immunohistochemistry. For indirect immunofluorescent staining, anti-p71-ATF-2 (#922, Cell Signaling), anti-p180/p182-p38 MAPK (#4631, Cell Signaling), anti-NeuN (MAB377, Chemicon), and TOTO-3 (Invitrogen) were used. The frozen sections were washed twice with Tris-buffered saline (144 mM NaCl, 10 mM Tris–HCl, pH 7.6) and incubated overnight at 4°C with primary antibody. Biotin-conjugated anti-rabbit IgG antibody served as the secondary antibody and was incubated at room temperature for 2 h and further incubated with streptavidin Alexa Fluor 488 (Molecular Probes) and Alexa Fluor 546 anti-mouse IgG at room temperature for 2 h.

Luciferase reporter assay

The *Htr5b* promoter-luciferase reporter, in which a 4.4 kb mouse *Htr5b* promoter DNA fragment (from −4182 to +243) was linked to the luciferase gene, was constructed. The mutant construct containing mutated CRE-like sites was constructed by replacing the 42-bp region containing the two CRE sites upstream (−3374 ∼ −3333) with the 6-bp sequence (GAGCTC) of a *Sac*I linker, whereas the 8-bp sequence of the third CRE site downstream (−2325 ∼ −2318) was replaced by the 8-bp sequence (AACGCGTT) of a *Mlu*I linker. To generate the ATF-7 expression vector, pact-ATF-7, the human ATF-7 cDNA was inserted into the chicken cytoplasmic β-actin promoter-containing vector. RN46A cells were cultured in Dulbecco's modified Eagle's medium (DMEM) and F-12 HAM (D8062, Sigma-Aldrich) (1:1 mixture) supplemented with 10% FBS at 33°C in 5% CO_2. RN46A cells were transfected using Lipofectamine Plus (Invitrogen) with 0.1 μg of the *Htr5b* promoter-luciferase reporter, various amounts of the ATF-7 expression plasmid or the control empty vector (0–3 μg), and 1 μg of the internal control pras-β-gal, in which the β-galactosidase gene was linked to the human c-*Ha-ras* promoter. At 48 h post-transfection, luciferase activity was measured and normalized for transfection efficiency by β-galactosidase activity.

ChIP assays

The brain tissues were prepared essentially as described by Tsankova *et al* (2004). The brainstem was removed by gross dissection, minced into ∼0.3 mm pieces, and immediately cross-linked in 1.5% formaldehyde for 15 min at room temperature. After addition of glycine to a final concentration of 0.125 M to quench the crosslinking reaction, the chromatin was solubilized and extracted with lysis buffer, and sheared to 400–600 bp fragments by sonication. ChIP assays were carried out essentially as described by Jin *et al* (2006). Immunoprecipitation was carried out for 4–10 h at 4°C with anti-ATF-7 (2F10 or 1A7), anti-histone H3 K9-m3 (ab8898, Abcam), anti-ESET (Upstate #07-378), or normal mouse or rabbit IgG as negative controls. The immunocomplexes were washed and incubated at 65°C in 100 μl of IP elution buffer (1% SDS, 0.1 M NaHCO₃, 250 mM NaCl, 200 μg/ml proteinase K, 10 mM DTT) to release proteins. The free precipitated DNA was further purified using a QIAquick PCR Purification Kit (Qiagen) and eluted in 30 μl sterile water. Eluted DNA samples were used for real-time PCR (7500 Real Time PCR System, Applied Biosystems). ChIP assays using RN46A cells were carried out essentially as described by Jin *et al* (2006). The primers and TaqMan probes (Qiagen) used for amplification are described in Supplementary Table S1.

Co-immunoprecipitation assay

For co-immunoprecipitation assays of endogenous ATF-7 and ESET, RN46A cells were lysed by mild sonication in NETN buffer (20 mM Tris–HCl, pH 8.0, 1 mM EDTA, 0.5% NP40, 400 mM NaCl). Lysates were immunoprecipitated using anti-ATF-7 (1A7) or control IgG. Immunocomplexes were resolved on 10% SDS polyacrylamide gels, and analyzed by western blotting with anti-ESET (Upstate #07-378).

Supplementary data

Supplementary data are available at *The EMBO Journal* Online (http://www.embojournal.org).

Acknowledgements

Conflict of interest

The authors declare that they have no conflict of interest.

References

Agelopoulos M, Thanos D (2006) Epigenetic determination of a cell-specific gene expression program by ATF-2 and the histone variant macroH2A. *EMBO J* **25:** 4843–4853

Artigasa F, Romeroa L, de Montignyb C, Blierb P (1996) Acceleration of the effect of selected antidepressant drugs in major depression by 5-HT1A antagonists. *Trends Neurosci* **19:** 378–383

Bibancos T, Jardim DL, Aneas I, Chiavegatto S (2007) Social isolation and expression of serotonergic neurotransmission-related genes in several brain areas of male mice. *Genes Brain Behav* **6:** 529–539

Blanc G, Hervé D, Simon H, Lisoprawski A, Glowinski J, Tassin JP (1980) Response to stress of mesocortico-frontal dopaminergic neurones in rats after long-term isolation. *Nature* **284:** 265–267

Blanchard RJ, McKittrick CR, Blanchard DC (2001) Animal models of social stress: effects on behavior and brain neurochemical systems. *Physiol Behav* **73:** 261–271

Boess FG, Martin IL (1994) Molecular biology of 5-HT receptors. *Neuropharmacology* **33:** 275–317

Breitwieser W, Lyons S, Flenniken AM, Ashton G, Bruder G, Willington M, Lacaud G, Kouskoff V, Jones N (2007) Feedback regulation of p38 activity via ATF2 is essential for survival of embryonic liver cells. *Genes Dev* **21:** 2069–2082

Brinkman BM, Telliez JB, Schievella AR, Lin LL, Goldfeld AE (1999) Engagement of tumor necrosis factor (TNF) receptor 1 leads to ATF-2- and p38 mitogen-activated protein kinase-dependent TNF-α gene expression. *J Biol Chem* **274:** 30882–30886

Chatton B, Bocco JL, Goetz J, Gaire M, Lutz Y, Kedinger C (1994) Jun and Fos heterodimerize with ATFa, a member of the ATF/CREB family and modulate its transcriptional activity. *Oncogene* **9:** 375–385

Connor TJ, Leonard BE (1998) Depression, stress and immunological activation: The role of cytokines in depressive disorders. *Life Sci* **62:** 583–606

Davis RJ (2000) Signal transduction by the JNK group of MAP kinases. *Cell* **103:** 239–252

De Graeve F, Bahr A, Chatton B, Kedinger C (2000) A murine ATFa-associated factor with transcriptional repressing activity. *Oncogene* **19:** 1807–1819

De Graeve F, Bahr A, Sabapathy KT, Hauss C, Wagner EF, Kedinger C, Chatton B (1999) Role of the ATFa/JNK2 complex in Jun activation. *Oncogene* **18:** 3491–3500

Egashira N, Tanoue A, Higashihara F, Fuchigami H, Sano K, Mishima K, Fukue Y, Nagai H, Takano Y, Tsujimoto G, Stemmelin J, Griebel G, Iwasaki K, Ikeda T, Nishimura R, Fujiwara M (2005) Disruption of the prepulse inhibition of the startle reflex in vasopressin V1b receptor knockout mice: reversal by antipsychotic drugs. *Neuropsychopharmacology* **30:** 1996–2005

Gaire M, Chatton B, Kedinger C (1990) Isolation and characterization of two novel, closely related ATF cDNA clones from HeLa cells. *Nucleic Acids Res* **18:** 3467–3473

Geyer MA, Krebs-Thomson K, Braff DL, Swerdlow NR (2001) Pharmacological studies of prepulse inhibition models of sensorimotor gating deficits in schizophrenia: a decade in review. *Psychopharmacology* **156:** 117–154

Geyer MA, Swerdlow NR, Mansbach RS, Braff DL (1990) Startle response models of sensorimotor gating and habituation deficits in schizophrenia. *Brain Res Bull* **25:** 485–498

Goetz J, Chatton B, Mattei MG, Kedinger C (1996) Structure and expression of the ATFa gene. *J Biol Chem* **271:** 29589–29598

Grailhe R, Grabtree GW, Hen R (2001) Human 5-HT(5) receptors: the 5-HT(5A) receptor is functional but the 5-HT(5B) receptor was lost during mammalian evolution. *Eur J Pharmacol* **418:** 157–167

Grailhe R, Waeber C, Dulawa SC, Hornung JP, Zhuang X, Brunner D, Geyer MA, Hen R (1999) Increased exploratory activity and altered response to LSD in mice lacking the 5-HT(5A) receptor. *Neuron* **22:** 581–591

Gupta S, Campbell D, Dérijard B, Davis RJ (1995) Transcription factor ATF2 regulation by the JNK signal transduction pathway. *Science* **267:** 389–393

Hai TW, Liu F, Coukos WJ, Green MR (1989) Transcription factor ATF cDNA clones: an extensive family of leucine zipper proteins able to selectively form DNA-binding heterodimers. *Genes Dev* **3:** 2083–2090

Jenck F, Moreau JL, Berendsen HH, Boes M, Broekkamp CL, Martin JR, Wichmann J, Van Delft AM (1998) Antiaversive effects of 5HT2C receptor agonists and fluoxetine in a model of panic-like anxiety in rats. *Eur Neuropsychopharmacol* **8:** 161–168

Jia S, Noma K, Grewal SI (2004) RNAi-independent heterochromatin nucleation by the stress-activated ATF/CREB family proteins. *Science* **304:** 1971–1976

Jin W, Takagi T, Kanesashi SN, Kurahashi T, Nomura T, Harada J, Ishii S (2006) Schnurri-2 controls BMP-dependent adipogenesis via interaction with Smad proteins. *Dev Cell* **10:** 461–471

Kaufer D, Friedman A, Seidman S, Soreq H (1998) Acute stress facilitates long-lasting changes in cholinergic gene expression. *Nature* **393:** 373–377

Livingstone C, Patel G, Jones N (1997) ATF-2 contains a phosphorylation-dependent transcriptional activation domain. *EMBO J* **14:** 1785–1797

Maekawa T, Bernier F, Sato M, Nomura S, Singh M, Inoue Y, Tokunaga T, Imai H, Yokoyama M, Reimold A, Glimcher LH, Ishii S (1999) Mouse ATF-2 null mutants display features of a severe type of meconium aspiration syndrome. *J Biol Chem* **274:** 17813–17819

Maekawa T, Sakura H, Kanei-Ishii C, Sudo T, Yoshimura T, Fujisawa J, Yoshida M, Ishii S (1989) Leucine zipper structure of the protein CRE-BP1 binding to the cyclic AMP response element in brain. *EMBO J* **8:** 2023–2028

Maekawa T, Shinagawa T, Sano Y, Sakuma T, Nomura S, Nagasaki K, Miki Y, Saito-Ohara F, Inazawa J, Kohno T, Yokota J, Ishii S (2007) Reduced levels of ATF-2 predispose mice to mammary tumors. *Mol Cell Biol* **27:** 1730–1744

Ng RK, Gurdon JB (2008) Epigenetic memory of an active gene state depends on histone H3.3 incorporation into chromatin in the absence of transcription. *Nat Cell Biol* **10:** 102–109

Nomura N, Zu YL, Maekawa T, Tabata S, Akiyama T, Ishii S (1993) Isolation and characterization of a novel member of the gene family encoding the cAMP response element-binding protein CRE-BP1. *J Biol Chem* **268:** 4259–4266

Paykel ES, Emms EM, Fletcher J, Rassaby ES (1980) Life events and social support in puerperal depression. *Br J Psychiatry* **136:** 339–346

Plassat JL, Boschert U, Amlaiky N, Hen R (1992) The mouse 5HT5 receptor reveals a remarkable heterogeneity within the 5HT$_{1D}$ receptor family. *EMBO J* **11:** 4779–4786

Rodgers RJ, Cole JC (1993) Influence of social isolation, gender, strain, and prior novelty on plus-maze behaviour in mice. *Physiol Behav* **54:** 729–736

Sano Y, Harada J, Tashiro S, Gotoh-Mandeville R, Maekawa T, Ishii S (1999) ATF-2 is a common nuclear target of Smad and TAK1 pathways in transforming growth factor-β signaling. *J Biol Chem* **274:** 8949–8957

Serrats J, Raurich A, Vilaró MT, Mengod G, Cortés R (2004) 5-HT5B receptor mRNA in the raphe nuclei: coexpression with serotonin transporter. *Synapse* **51:** 102–111

Spooren WP, Vassout A, Neijt HC, Kuhn R, Gasparini F, Roux S, Porsolt RD, Gentsch C (2000) Anxiolytic-like effects of the prototypical metabotropic glutamate receptor 5 antagonist 2-methyl-6-(phenylethynyl)pyridine in rodents. *J Pharmacol Exp Ther* **295:** 1267–1275

Takeda J, Maekawa T, Sudo T, Seino Y, Imura H, Saito N, Tanaka C, Ishii S (1991) Expression of the CRE-BP1 transcriptional regulator binding to the cyclic AMP response element in central nervous system, regenerating liver, and human tumors. *Oncogene* **6:** 1009–1014

Tsankova NM, Kumar A, Nestler EJ (2004) Histone modifications at gene promoter regions in rat hippocampus after acute and chronic electroconvulsive seizures. *J Neurosci* **24:** 5603–5610

van Dam H, Wilhelm D, Herr I, Steffen A, Herrlich P, Angel P (1997) ATF-2 is preferentially activated by stress-activated protein kinases to mediate c-*jun* induction in response to genotoxic agents. *EMBO J* **14:** 31798–31811

Vergara C, Ramirez B (2004) CNTF, a pleiotropic cytokine: emphasis on its myotrophic role. *Brain Res Brain Res Rev* **47:** 161–173

Wang H, An W, Cao R, Xia L, Erdjument-Bromage H, Chatton B, Tempst P, Roeder RG, Zhang Y (2003) mAM facilitates conversion by ESET of dimethyl to trimethyl lysine 9 of histone H3 to cause transcriptional repression. *Mol Cell* **12:** 475–487

Wilkinson LS, Killcross SS, Humby T, Hall FS, Geyer MA, Robbins TW (1994) Social isolation in the rat produces developmentally specific deficits in prepulse inhibition of the acoustic startle response without disrupting latent inhibition. *Neuropsychopharmacology* **10:** 61–72

Wu W, Yamaura T, Murakami K, Ogasawara M, Hayashi K, Murata J, Saiki I (1999) Involvement of TNF-α in enhancement of invasion and metastasis of colon 26-L5 carcinoma cells in mice by social isolation stress. *Oncol Res* **11:** 461–469

Yamada K, Wada E, Yamano M, Sun YJ, Ohara-Imaizumi M, Nagamatsu S, Wada K (2002) Decreased marble burying behavior in female mice lacking neuromedin-B receptor (NMR-R) implies the involment of NMB/NMB-R in 5-HT neuron function. *Brain Res* **942:** 71–78